Draft version June 27, 2020
Typeset using LaTeX **preprint** style in AASTeX62

Empirical Dust Models

ChangHoon Hahn[1, 2, *] and IQ Collaboratory

[1] *Lawrence Berkeley National Laboratory, 1 Cyclotron Rd, Berkeley CA 94720, USA*
[2] *Berkeley Center for Cosmological Physics, University of California, Berkeley CA 94720, USA*

(Dated: `DRAFT --- 3628bb1 --- 2020-06-23 --- NOT READY FOR DISTRIBUTION`)

ABSTRACT

We construct a dust empirical model (DEM) framework for applying dust attenuation to simulated galaxies based on handful of sensible assumptions that come from our understanding of dust attenuation. The DEM framework is essentially based on state-of-the-art attenuation curves with a flexible parameterization that allows us to statistically sample them. Applying DEMs to three different hydrodynamic simulations, SIMBA, Illustris TNG, and EAGLE, we are able to produce UV and optical photometry consistent with SDSS observations ($(G-R)-M_r$ color-magnitude and $(FUV-NUV)-M_r$ relations). This suggests that there's enough freedom in our current understanding (or lack) of dust for all simulations to reproduce observations. Meanwhile, the DEM provides some insights into dust as well as the subgrid physics that goes into the hydro simulations.

Keywords: keyword1 – keyword2 – keyword3

1. INTRODUCTION

dust is important because....

assumptions on the attenuation curve can dramatically impact the physical properties inferred from SED fitting (*e.g.* Kriek & Conroy 2013; **?**; **?**; Salim & Narayanan 2020).

motivation for an empirical dust attenuation model

attenuation vs extinction. While extinction curves have been derived from observations and theoretically, it's not easy to map this to attenuation curves. Attenuation curves are a product of complicated empirical processes since it accounts for light that gets scattered and star light that is not obscured

This makes modeling them in a complete physically motivated method expensive. People have done it Narayanan et al. (2018); Trayford et al. (2020). some detail about the radiative transfer method and such. But besides being expensive they have to make a number of assumptions anyway. e.g. Narayanan et al. (2018) assumes a fixed extinction curve.

* hahn.changhoon@gmail.com

Moreover, because the radiative transfer method is expensive it's hard to compare many different simulations. Not only that, observables generated from simulations that take into radative transfer dust models complicates simulation to simulation comparisons. Because you're simultaneously comparing the galaxy formation prescription and all the dust prescription.

emphasize somewhere here that using a prescription trained one sim doesn't translate well to other sims.

Instead, we present a framework using flexible dust empirical models that paints attenuation curves onto galaxies. describe at a high level how we are parameterizing DEMs

emphasize comparisons in observable space (Nelson et al. (2018) talks about importance of color)

talk about the advantages: extremely flexible so it can encompass the wide variety of attenuation curves found in radiative transfer, easy to correlate the attenuation curve with galaxy properties.

Also DEMs make it possible to statistically apply attenuation curves for large galaxy population. Putting this ontop of simulations, we can use them to generate observables and compare them to observations to constrain the DEM. This framework allows us to learn about attenuation curves given a model for galaxy formation.

The other way around also works. If you don't care about dust at all, DEM provides a framework to easily marginalize over dust attenuation and treat dust as a nuisance parameter.

In this paper, we do above for multiple simulations.

Starkenburg et la. in prep will use this framework to marginalize over dust and compare galaxy populations predicted by multiple simulations .

CH: why do we only do centrals?

2. DATA

2.1. *SDSS DR7 Central Galaxies*

Throughout the paper we compare the simulations and models described below to the observed SDSS central galaxy sample from the Tinker et al. (2011) group catalog. The group catalog, first, selects volume-limited sample of galaxies at $z \approx 0.04$ with $M_r < -18$ and complete above $M_* > 10^{9.4} h^{-2} M_\odot$ from the NYU Value-Added Galaxy Catalog (VAGC; Blanton et al. 2005) of SDSS DR7 (Abazajian et al. 2009). The stellar masses are estimated using the `kcorrect` code (Blanton & Roweis 2007) assuming a Chabrier (2003) initial mass function.

Central galaxies are then identified using a halo-based group finder that uses the abundance matching ansatz to iteratively assign halo masses to groups. Every group contains one central galaxy, which by definition is the most massive, and a group can contain ≥ 0 satellites. As with any group finder, galaxies are misassigned due to projection effects and redshift space distortions; however, the central galaxy sample has a purity of ∼90% and completeness of ∼95% (Tinker et al. 2018).

2.2. *Illustris TNG*

describe what galaxy properties (SFH, ZH, etc) are available TODO

2.3. *SIMBA*

describe what galaxy properties (SFH, ZH, etc) are available TODO

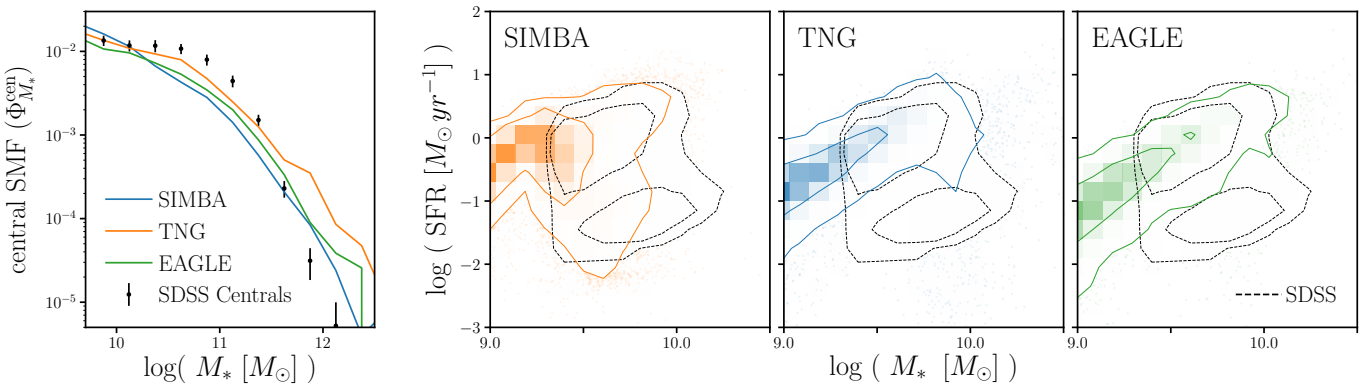

Figure 1. The stellar mass functions of central galaxies, $\Phi^{cen}_{M_*}$, of the SIMBA (orange) and TNG (blue) simulations compared to the SDSS $\Phi^{cen}_{M_*}$. The uncertainties for the SDSS $\Phi^{cen}_{M_*}$ are derived using jackknife resampling and SDSS centrals are identified using a halo-based group finder (Section 2.1). For SIMBA and TNG galaxies, we calculate M_* as the total stellar mass within the host halo, excluding contributions from any subhalos; centrals are classified based on their individual definition (Section 2.2 and 2.3). should we include total SMF...? *The simulations and observations have loosely consistent* $\Phi^{cen}_{M_*}$. The M_* – SFR relation of central galaxies in SIMBA (orange), TNG (blue), and EAGLE (green) simulations and SDSS observations. **CH:** describe where the M* and SFRs come from for everythign. The differences among the M_* – SFR relations demonstrate that the hydro simulations predict galaxy populations with significantly different physical properties.

In Figure **??**, we compare the stellar mass function (SMF) of our SDSS central galaxy sample along with central galaxy SMFs of the SIMBA (orange) and TNG (blue) simulations. The uncertainties for the SDSS SMF are derived from jackknife resampling. Although we present the SMFs for reference, we do not use stellar masses throughout the paper since they are inconsistently defined among simulations and observations. Instead, we compare between the simulations and SDSS using luminosity, M_r, which we consistently forward model and measure in the simulations. In these comparisons, we restrict ourselves to galaxies brighter than $M_r < -20$, where our SDSS central galaxy sample is complete.

instantaneous SFR=0 for $\sim 11\%$ of SIMBA galaxies, $\sim 13\%$ for TNG, $\sim 2\%$ for EAGLE

2.4. *Spectral Energy Distributions*

describe how the SED is generated using the SFH and ZHs TODO

2.5. *Forward Modeling Optical and UV photometry*

Trayford et al. (2015) Figure 1.a. has a comparison without dust that's roughly consistent with what we find for EAGLE

3. DUST EMPIRICAL MODELING

3.1. *Fiducial DEM*

motivation for the DEM model TODO

Trayford et al. (2015) uses an empirical dust model but doesn't implement an attenuation curve but rather multiplicative factors for the broadband photometry.

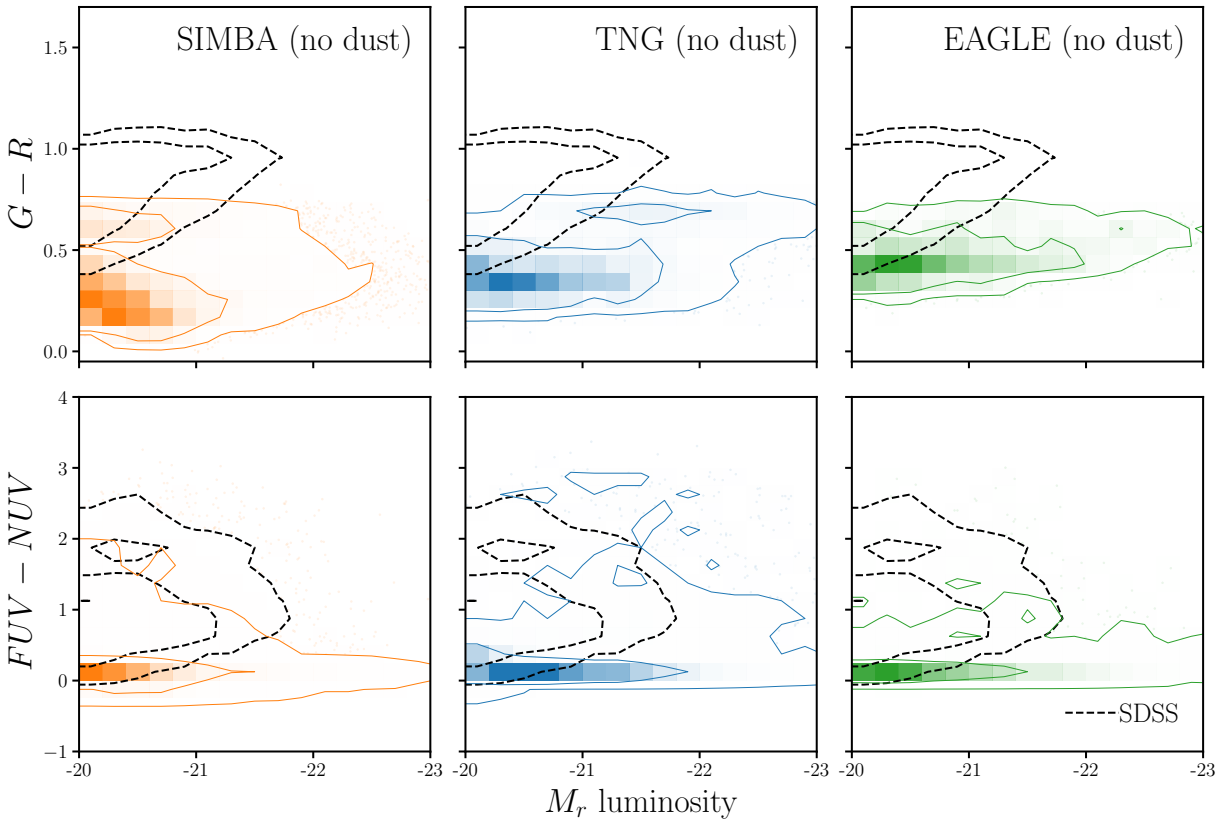

Figure 2. We present the distributions of the main observables used throughout the paper for SDSS (left), SIMBA (center), and TNG (right) centrals. We do *not* include any prescription for dust for the simulated galaxies. The top panels present the $G-R$ versus M_r color magnitude relations while the bottom panels present the $FUV-NUV$ versus M_r relations. The observables for the SIMBA and TNG simulated galaxies are derived using forward modeling and are therefore consistent with SDSS measurements (Section 2.5). The contours for SIMBA and TNG do not include galaxies with SFR= 0, which we mark separately in black. Despite similar SMFs, *the simulations without any dust prescription show stark differences with observations in the color-magnitude observable-space.*

We begin by defining the dust attenuation curve $A(\lambda)$ as

$$F_o(\lambda) = F_i(\lambda) 10^{-0.4A(\lambda)} \tag{1}$$

where F_o is the observed flux and F_i is the intrinsic flux. We normalize the attenuation at the V band,

$$A(\lambda) = A_V \frac{k(\lambda)}{k_V}. \tag{2}$$

For the normalization of the attenuation curve, A_V, we use the slab model from Somerville & Primack (1999); Somerville et al. (2012). In the slab model the amplitude of attuenuation depends on the inclination angle, i, and the optical depth, τ_V:

$$A_V = -2.5 \log \left[\frac{1 - e^{-\tau_V \sec i}}{\tau_V \sec i} \right] \tag{3}$$

justification of why this is enough. We sample i uniformly. TODO

Recently, Salim & Narayanan (2020) find significant dependence in A_V on both M_* and SFR. We include this dependence through τ_V, which we flexibly parameterize as

$$\tau_V(M_*, \mathrm{SFR}) = m_{\tau,1} \log\left(\frac{M_*}{10^{10} M_\odot}\right) + m_{\tau,2} \log \mathrm{SFR} + c_\tau. \tag{4}$$

Next, for the wavelength dependence of the attenuation curve, we use $k(\lambda)$ from Noll et al. (2009):

$$k(\lambda) = (k_{\mathrm{Cal}}(\lambda) + D(\lambda)) \left(\frac{\lambda}{\lambda_V}\right)^{\delta}. \tag{5}$$

Here $k_{\mathrm{Cal}}(\lambda)$ is the Calzetti (2001) curve:

$$k_{\mathrm{Cal}}(\lambda) = \begin{cases} 2.659(-1.857 + 1.040/\lambda) + R_V, & 6300\mathring{A} \leq \lambda \leq 22000\mathring{A} \\ 2.659(-2.156 + 1.509/\lambda - 0.198/\lambda^2 + 0.011/\lambda^3) + R_V & 1200\mathring{A} \leq \lambda \leq 6300\mathring{A} \end{cases}$$

where λ_V is the V band wavelength. δ, the slope of the attenuation curve. also correlates with galaxy properties. So we parameterize δ and

$$\delta(M_*, \mathrm{SFR}) = m_{\delta,2} \log\left(\frac{M_*}{10^{10} M_\odot}\right) + m_{\delta,2} \log \mathrm{SFR} + c_\delta \tag{6}$$

$D(\lambda)$ is the UV dust bump, which we parameter using the standard Lorentzian-like Drude profile:

$$D(\lambda) = \frac{E_b (\lambda \Delta\lambda)^2}{(\lambda^2 - \lambda_0^2)^2 + (\lambda \Delta\lambda)^2} \tag{7}$$

where λ_0, $\Delta\lambda$, and E_b are the central wavelength, FWHM, and strength of the bump, respecitvely. In our DEM, we assume fixed $\lambda_0 = 2175\mathring{A}$ and $\Delta\lambda = 350\mathring{A}$.

Kriek & Conroy (2013) and Tress et al. (2018) found evidence that E_b correlates with the slope of the attenuation curve for star-forming galaxies $z \sim 2$. This was dependence was confirmed with simulations in **?**. E_b:

$$E_b = m_E \ \delta + c_E \tag{8}$$

we fixed this and find our results do not change significantly. TODO

We also split the attenuation on the star light and nebular emission

$$F_o(\lambda) = F_i^{\mathrm{star}}(\lambda) 10^{-0.4A(\lambda)} + F_i^{\mathrm{neb}}(\lambda) 10^{-0.4A_{\mathrm{neb}}(\lambda)} \tag{9}$$

where we parameterize

$$A_{\mathrm{neb}}(\lambda) = f_{\mathrm{neb}} A(\lambda) \tag{10}$$

mention of how we treat SFR = 0 galaxies TODO

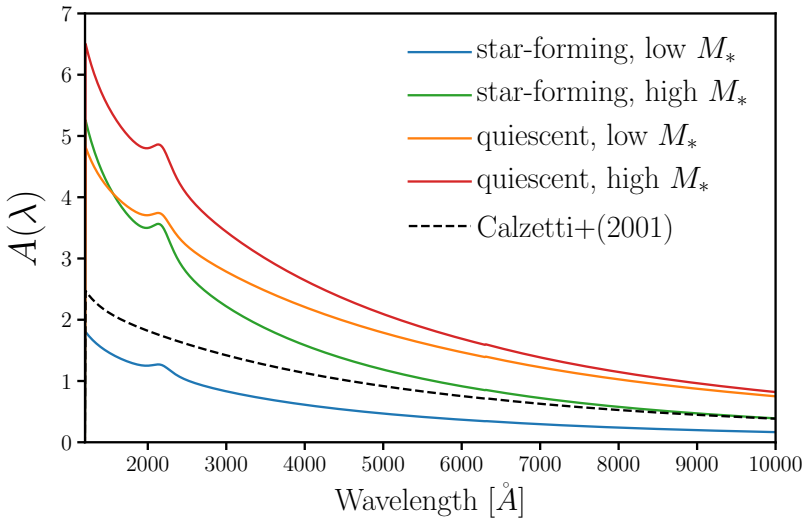

Figure 3. Comparison of the attenuation curve for our fiducial dust empirical model (DEM; black) to common attenuation curves in the literature (Calzetti 2001, orange; Salim et al. 2018, blue). We compare the curves for typical star-forming galaxies with SFR $= 10^{0.5} M_\odot/yr$ in the left panel and for quiescent galaxies with SFR $= 10^{-2} M_\odot/yr$ in the right. For our fiducial DEM, we use parameter values at the center of the priors listed in Table 1 and include attenuation curves for $M_* = 10^{9.5}$ (dashed) and $10^{11} M_\odot$ (solid). *Our fiducial DEM is flexibly parameterized to incorporate both M_* and SFR dependence in the attenuation curve* (Section 3.1).

Table 1. Parameters of the Dust Empirical Models

Parameter	Definition	prior
m_{τ,M_*}	Slope of the $\log M_*$ dependence of optical depth, τ_V	flat $[-5., 5.]$
$m_{\tau,\mathrm{SFR}}$	Slope of the $\log \mathrm{SFR}$ dependence of optical depth, τ_V	flat $[-5., 5.]$
c_τ	amplitude of the optical depth, τ_V	flat $[0., 6.]$
$m_{\delta,1}$	Slope of the $\log M_*$ dependence of the attenuation curve slope offset, δ	flat $[-4., 4.]$
$m_{\delta,2}$	Slope of the $\log \mathrm{SFR}$ dependence of the attenuation curve slope offset, δ	flat $[-4., 4.]$
c_δ	amplitude of the attenuation curve slope offset, δ	flat $[-4., 4.]$
f_{neb}	fraction of nebular attenuation curve	flat $[1., 4.]$

3.2. *Likelihood-Free Inference*

Approximate Bayesian Computation with Population Monte Carlo Hahn et al. (2017),

To compare the outputs of our DEMs to observations, we first measure the color-magnitude observables ($G-R$, $FUV-NUV$, and M_r) as described in Section 2.5 consistent with SDSS measurements. Afterwards, we compare the forward modeled observables to SDSS using a L2 norm distance metric:

$$\bar{\rho}(\theta) = \sum_{i=1}^{n} \left[X_i^{\rm SDSS} - X_i^{\rm model}(\theta)\right]^2 . \quad (11)$$

$X^{\rm SDSS}$ and $X^{\rm model}(\theta)$ are n-dimensional data vectors of the SDSS and model observables. In our case, we use a 3-dimensional histogram along $G-R$, $FUV-NUV$,

Ishida et al. (2015)

Paragraph on the priors we choose.

- flat priors on everything. We might want to note that this doesn't give flat priors on τ_V or μ_{A_V} and σ_{A_V} for NT but we're ultimately interested in the dependence.
- priors were chosen to be uniformative and encompass constraints in the literature:
- m_E and c_E were chosen to be include Kriek & Conroy (2013); Narayanan et al. (2018); Tress et al. (2018)

4. RESULTS

We present the posterior distributions of the DEM parameters for the SIMBA (orange), TNG (blue), and EAGLE (green) hydro simulations in Figure 4. The DEM parameters include m_{τ,M_*}, $m_{\tau,\rm SFR}$, and c_τ, which parameterize the M_* dependence, SFR dependence, and amplitude of τ_V, the V-band optical depth. τ_V dictates the overall strength of the dust attenuation. They also include m_{δ,M_*}, $m_{\delta,\rm SFR}$, and c_δ, which parameterize the M_* dependence, SFR dependence, and amplitude of δ, the slope offset of the attenuation curve (Section 3.1 and Table 1). The posteriors are derived using ABC (Section 3.2) and the contours mark the 68% and 95% confidence intervals.

In addition, we present the observables predicted by the DEM with median of the posteriors for the SIMBA (orange), TNG (blue), and EAGLE (green) simulations in Figure 5. We include the SDSS observables for comparison (black dashed; Section 2.1). The top panels present the $(G-R)-M_r$ color-magnitude relations while the bottom panels present the $(FUV-NUV)-M_r$ relations. Without any dust prescriptions, we found that simulations predict dramatically different observables than SDSS (Figure 2). **CH:** something about clear bimodality with the red sequence and blue cloud In contrast, *using DEMs we produce* $(G-R)-M_r$ *and* $(FUV-NUV)-M_r$ *relations consistent with SDSS for all of the simulations.*

We examine the observables more closely in Figure 6, where we present the $G-R$ (left) and $FUV-NUV$ (right) distributions in M_r bins for the DEM models of the SIMBA (orange), TNG (blue), and EAGLE (green) simulations. The top panels contain galaxies with $-20 > M_r > -21$ and the bottom panels contain galaxies with $-21 > M_r > -22.5$. In each panel we include the SDSS distributions for comparison (grey shaded). These distributions are number densities. The positions of the red sequence and blue cloud in the $G-R$ distributions for the DEM models are consistent with the SDSS distribution. They also produce FUV_NUV distributions with peaks consistent with observations. We also find good agreement in the overall normalization (number density), especially for the $-20 > M_r > -21$ bin.

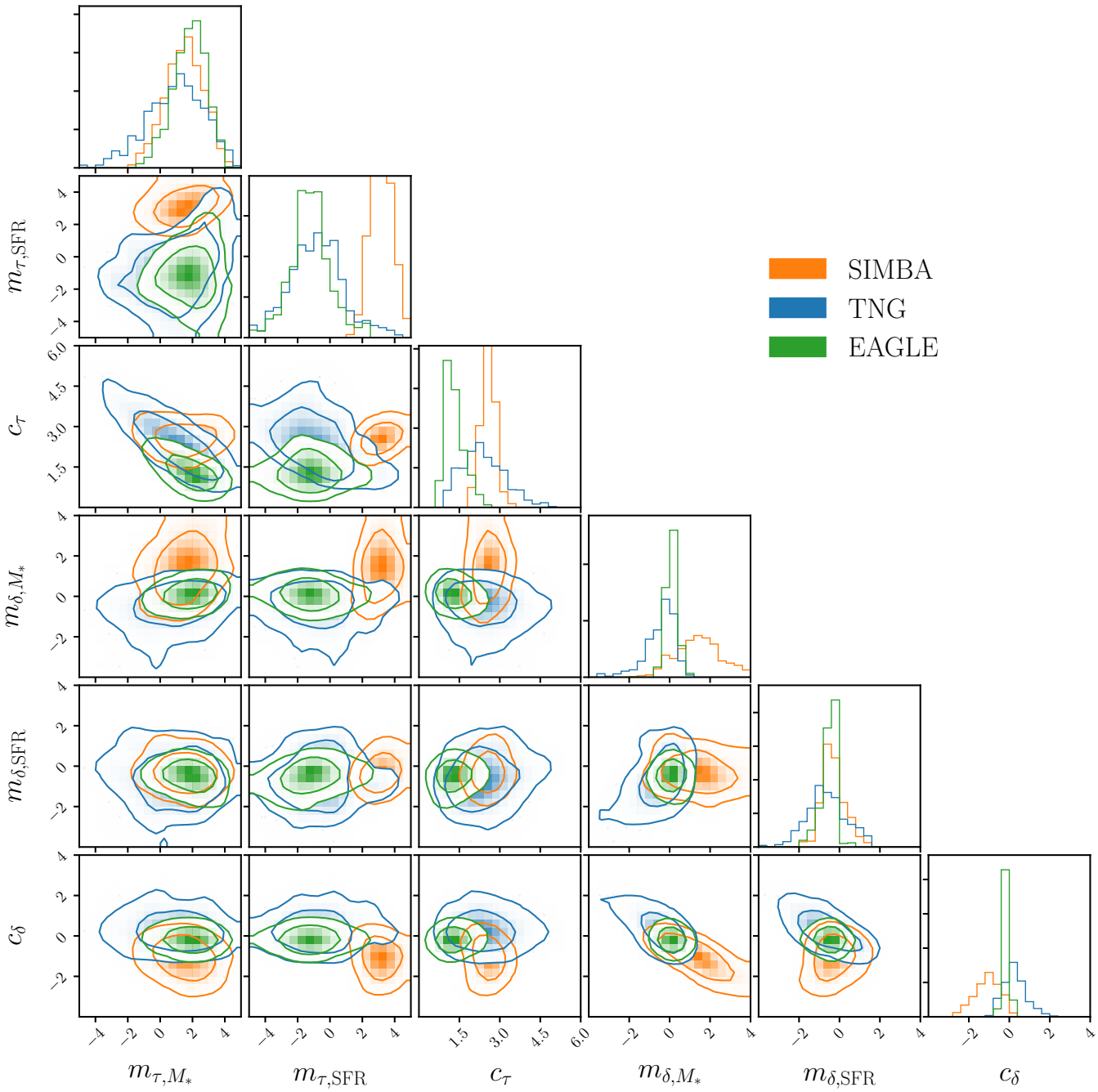

Figure 4. Posterior distributions of our DEM parameters for the SIMBA (orange), TNG (blue), and EAGLE (green) hydro simulations. The contours mark the 68% and 95% confidence intervals. We describe the parameters in Section 3.1 and Table 1 and derive these posteriors using Approximate Bayesian Computation (Section 3.2). In all simulations, dust attenuation increases for higher M_* galaxies ($m_{\tau,M_*} \sim 2$). The simulations also have consistent optical depth amplitudes (c_τ). However, the SFR dependence of τ_V is different among the simulations. For TNG and EAGLE, star-forming galaxies have lower τ_V; for SIMBA quiescent galaxies have lower τ_V. Meanwhile, for the slope offset of the attenuation curve, δ, we find little M_* and SFR dependence in the simulations and that the amplitude (c_τ) is consistent with 0.

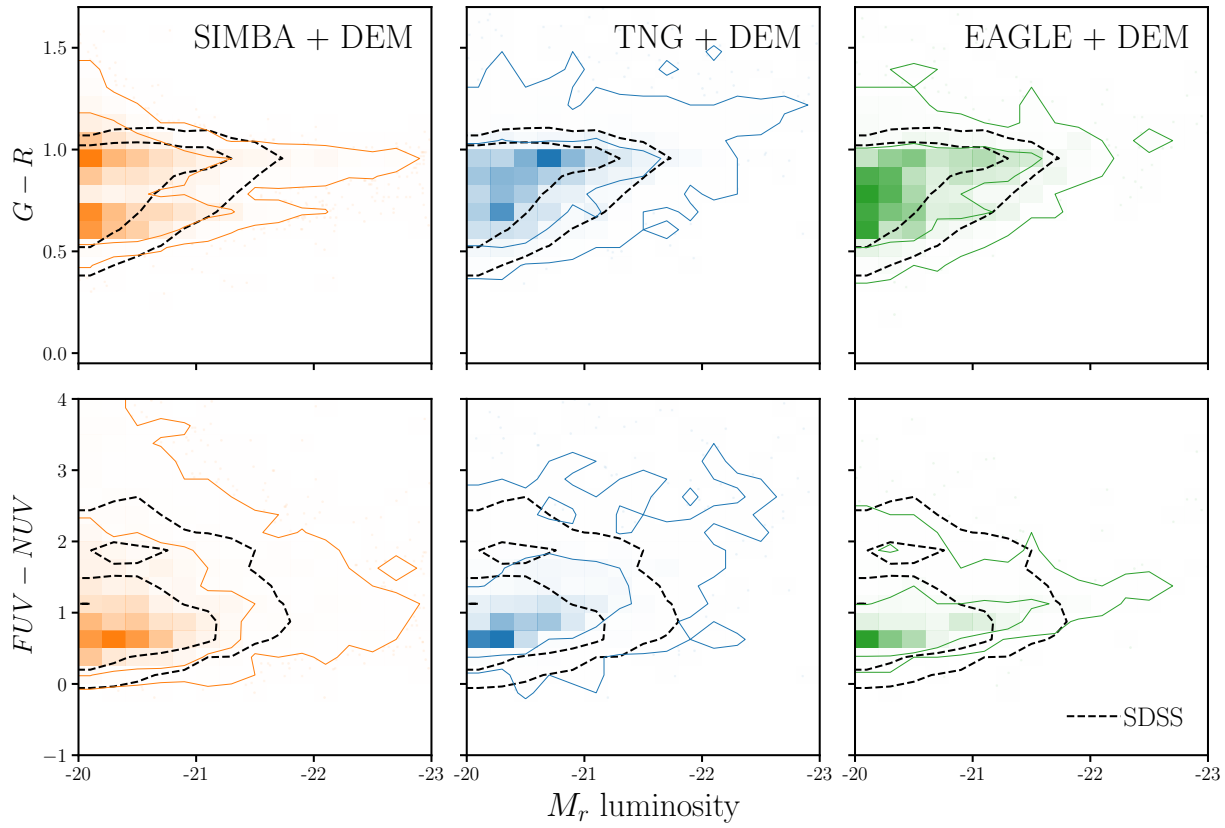

Figure 5. $(G-R)-M_r$ color-magnitude (top panels) and $(FUV-NUV)-M_r$ (bottom panels) relations predicted by the median DEM posteriors for the SIMBA (orange), TNG (blue), and EAGLE (green) hydro simulations. For comparison, we include the observables for SDSS in the left-most panel (Section 2.1). The median posterior DEMs produce dramatically different observables than when we do not include any dust prescription (Figure 2). Hence, dust must be account for when interpreting and comparing simulations. Moreover, with the DEMs, all three simulations produce observables consistent with SDSS. Since different simulations can produce reproduce observations by varying dust, dust significantly limits our ability to constrain the physical processes that go into galaxy simulations.

There are also a few discrepancies between the DEM models and SDSS observations. First, the red sequence in the observed $G-R$ distribution has a sharp red color cut-off. In contrast, we do not find as sharp of a $G-R$ cut off in the DEM models, and find a small fraction of galaxies redder than observations. Furthermore, while the DEM models for TNG and EAGLE agree with SDSS, the DEM model for SIMBA overpredicts blue galaxies. **CH:** what do we want to do with SIMBA? We also find that the TNG and EAGLE DEM models slightly overpredict galaxies in the higher luminosity bin and produce a broader $G-R$ distribution. Nonetheless, Figure 6 demonstrates that overall the DEM models for SIMBA, TNG, and EAGLE produce observables are in good agreement with SDSS.

Previous works in the literature have also presented models that predict colors and luminosities for different simulations and dust models and compared them to observations. For instance, Trayford et al. (2015) calculate colors and luminosities for $z = 0.1$ galaxies using EAGLE with the GALAXEV population synthesis models and a two-component screen model for dust. Compared to GAMA obser-

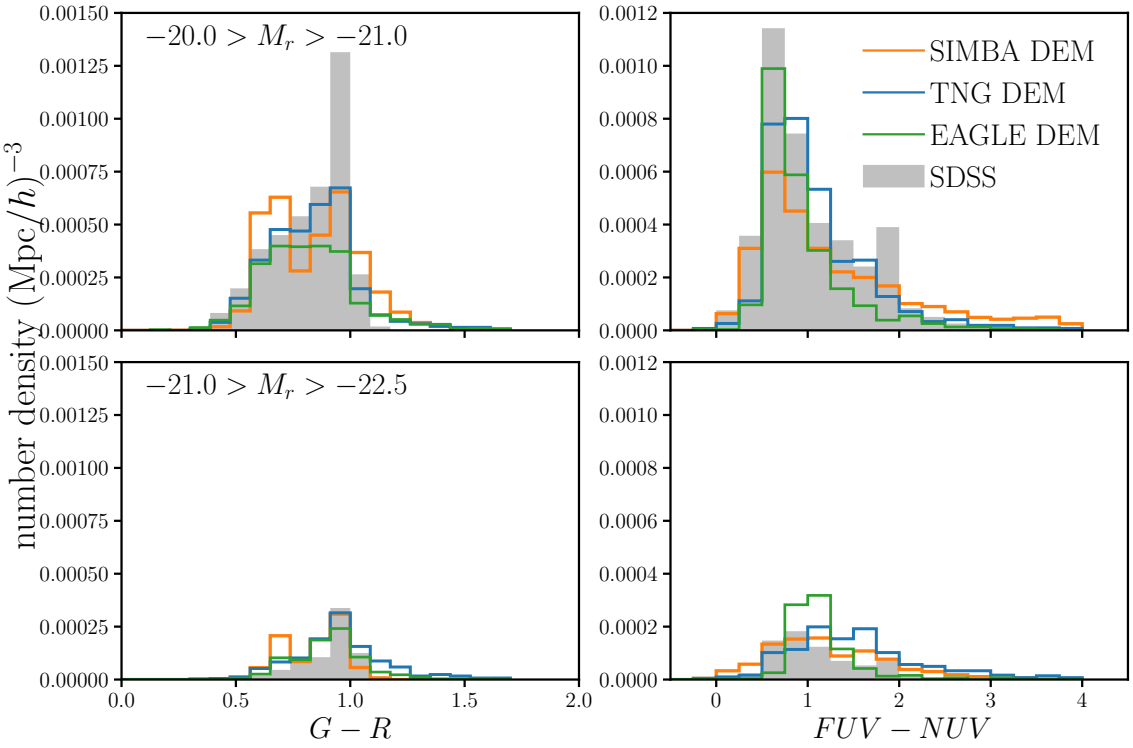

Figure 6. $G - R$ (left) and $FUV - NUV$ (right) number density distributions for the DEM models of the SIMBA (orange), TNG (blue), and EAGLE (green) simulations in two M_r bins: $-20 > M_r > -21$ (top panels) and $-21 > M_r > -22.5$ (bottom panels). Each of the DEM models are run using the median posterior parameter values. In comparison to SDSS (grey shaded), the DEM models predict consistent red sequence and blue cloud positions in the $G - R$ distributions, $FUV - NUV$ peak positions, and number density. *Overall the DEM models for SIMBA, TNG, and EAGLE produce observables are in good agreement with SDSS.*

vations, their model produces a bluer red sequence and overpredicts luminous blue galaxies (Trayford et al. 2015, Figure 5). Although a detailed comparison is difficult since they compare all galaxies, not just centrals, we note that the DEM models find good agreement in the positions of the red sequences. Furthermore, for TNG and EAGLE, the DEM models do not overpredict blue galaxies. Even for SIMBA, the DEM model overpredict blue galaxies by a smaller amount.

More recently, Trayford et al. (2017) calculated optical colors for the EAGLE simulation using SKIRT, a Monte Carlo radiative transfer code (Camps & Baes 2015), to model the dust. Trayford et al. (2017) compares all galaxies so again, we do not include a direct comparison. Compared to GAMA, while they find good agreement with observations at intermediate masses, $10^{10.5} < M_* < 10^{10.8} M_\odot$, they again find a bluer red-sequence at $10^{11.2} < M_* < 10^{11.5}$. While we do not present comparisons in M_* bins, which compare SED derived M_* to the predicted M_* from simulations, we find that the position of the red sequence in the DEM models are in good agreement with SDSS even at $M_* > 10^{11.2}$. Our models, however, predict an overall broader color distribution at the high mass end. Using the same Trayford et al. (2017) EAGLE and SKIRT framework, Baes et al. (2019) compared the predicted cosmic spectral energy distributions (CSED) to observations. While this

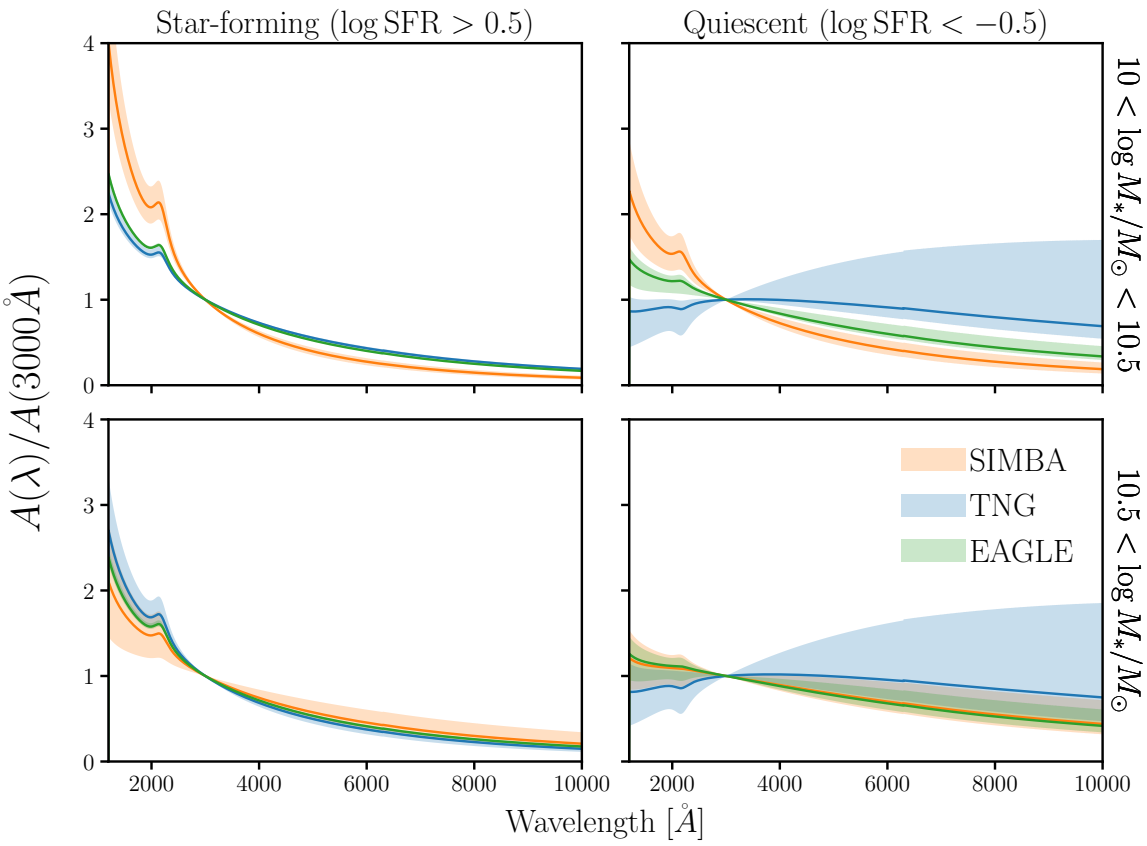

Figure 7.

comparison averages over the galaxy populations, they find the EAGLE-SKIRT CSED overestimates the observed CSED in the UV regime. Moreover, the $FUV-NUV$ color of their CSED is significantly higher than GAMA $FUV-NUV$. The DEM models on the other hand, predict $FUV-NUV$ in good agreement with observations.

Besides with EAGLE, Nelson et al. (2018) calculated optical colors for the TNG simulations with a dust model that includes attenuation due to dense gas birth clouds surrounding young stellar populations and also attenuation due to simulated distribution of neutral gas and metals. Although they compare the color distribution for all galaxies in bins of M_*, so we cannot directly compare to the DEM models, compared to SDSS they find bluer red sequence peak position and narrower blue cloud. We find neither of these discrepancies between the DEM models and SDSS. **CH:** restatement of how the DEM models have the flexibility to reproduce the optical and UV color-magnitude relationship.

The simulations with DEMs predict observables in agreement with observations despite the significant differents in the SMFs and M_*-SFR relations (Figure **??**). In other words, the DEM has the flexiblity to reproduce observations even when simulations predict galaxy populations with significantly different physical properties. We emphasize that the DEM is based on the standard prescriptions for dust attenuation and, thus, serve as a flexible parameterization within the bounds of our current understanding of dust in galaxies.

Figures 5 and 6 highlights two key points. First, any comparison of simulations must account for dust. Dust entirely changes the predictions of simulations in observables-space. Without dust, we did not find bimodality in the color-magnitude relation. Fortunately, the DEM provides a simple framework for including dust motivated by attenuation laws and correlations with the physical properties of galaxies. Second, the current limiations in our understanding of dust in galaxies significant impedes our ability to understand galaxy formation from simulations. To robustly interpret any comparison of simulations, we would need to marginalize over dust (*e.g.* DEM parameters). Since DEMs can produce consistent observables for a range of simulations, marginalizing over dust would leave little constraining power on the subgrid prescriptions (*i.e.* galaxy physics) of the simulations.

The DEMs demonstrate that simulations can closely match observations by varying dust attenuation. They therefore illustrate how dust is a major bottleneck for directly interpreting galaxy simulations for insights into galaxy formation. In addition, DEMs also provide some insight into dust. Given our parameterization (Section 3.1), it is especially easy to interpret correlation between dust attenuation and galaxy physical properties. For instance, the posteriors of DEM parameters in Figure 4 reveal a number of consistent trends across the simulations. In all three simulations, we find significant positive M_* dependence of τ_V: $m_{\tau,M_*} \sim 2$. Regardless of the underlying hydro simulations, we find that *galaxies with higher M_* have overall higher dust attenuation.*

This M_* dependence is consistent with prevoius works in the literature. The seminal work of Burgarella et al. (2005), for instance, found significant positive M_* dependence in FUV attenuation in NUV-selected and FIR-selected samples of Buat et al. (2005) and Iglesias-Páramo et al. (2006). Garn & Best (2010) also find positive M_* dependence in Balmer decrement-based Hα attenuation in $\sim$90,000 SDSS star-forming galaxies. Battisti et al. (2016) similarly find higher Balmer optical depth for higher M_* in $\sim$10,000 star-forming galaxies from GALEX and SDSS. Most recently, Salim et al. (2018) find higher V and FUV attenuation for more masssive star-forming galaxies in the GALEX-SDSS-WISE Legacy Catalog 2 (GSWLC2). citation is a bit SDSS heavy. Anything else in the literature? TODO

In addition to the M_* dependence, the DEM posteriors also allow us to examine the correlation bteween dust attenuation and star formation. For TNG and EAGLE, we infer DEM posteriors with $m_{\tau,\mathrm{SFR}} \sim -1$ (Figure 4). This means that TNG and EAGLE require higher attenuation for galaxies with lower SFR — *i.e.* quiescent galaxies have higher dust attenuation overall. While previous works that have examined the relationship between dust attenuation and SFR in observations (*e.g.* Garn & Best 2010; **?**; Battisti et al. 2016, 2017), they focus solely on star-forming galaxies. While they find that star-forming galaxies with higher SFR have higher attenuation, much of this trend is driven by the star-forming sequence (more massive star-forming galaxies have higher SFR; Garn & Best 2010; Battisti et al. 2017). At fixed M_*, observations find no strong SFR dependence for the SF population.

For SIMBA, unlike for TNG and EAGLE, we infer $m_{\tau,\mathrm{SFR}} \sim 3$: galaxies with higher SFR have higher dust attenuation (Figure 4). In fact, the attenuation is so high for star-forming galaxies that they populate the red sequence rather than the blue cloud in the color-magnitude relation. This extreme SFR dependence in the dust attenuation that results in a contradiction of established color-SFR relations, is due to the fact that SIMBA predicts a population of star-forming with exceptionally

high SFR, that seemingly lie above the SFS (Figure 1). In a SIMBA DEM model with $m_{\tau,\mathrm{SFR}} < 0$, these high SFR galaxies would be high luminosity blue galaxies, not found in observations. **CH:** If we impose a $m_{\tau,\mathrm{SFR}} < 0$ prior for the SIMBA DEM model, we struggle to reproduce observables consistent with SDSS. The difference in $m_{\tau,\mathrm{SFR}}$ among the hydro simulations demonstrates that, in addition to insights on dust in galaxies, our DEM approach can also highlights differences and limiations among simulations. Moreover, it further highlights that dust attenuation can be adjusted, within priors set by observations, so that any simulation can match observations.

In addition to the M_* and SFR dependence, our results also shed light on dust attenuation in quiescent galaxies, which is difficult to measure from observations. For non-star-forming galaxies, MIR emission from active galactic nuclei (AGN) heating nearby dust complicate methods that rely on IR luminosity to measure dust attenuation. Even SED fitting methods require accounting for AGN MIR emission (**??**Salim et al. 2018). Since we utilize a forward modeling approach with optical and UV data, we don't have this issue. **CH:** what do we learn about quiescent galaxy attenuation?

CH: delta - galaxy property connection We also find overall little M_* and SFR dependence in δ. In fact, the amplitude of δ is roughly consistent with 0. This is consistent with Salim & Narayanan (2020), where they measured the attenuation curve slopes of $23,000$ galaxies from GALEX-SDSS-WISE Legacy Catalog 2 (**CH:** cite). comparison to **?** (only 129 nearby galaxies though) **?** (one galaxy, jesus) Kriek & Conroy (2013) using stacked SEDs of medium- and broadband photometry of galaxies at 0.5 ¡ z ¡ 2 find an average slope of delta=-0.2 .

CH: can we say anything about the $A_V - \delta$ relation?

CH: variation of attenuation curves While an empirical prescription like DEM doesn't allow explicit modeling of the complex dust-star geometry, it does a good job at mimicking it. **CH:** how does this compare to the literature? comparison to Narayanan et al. (2018) paper comparison to Salim et al. (2018) for SF population comparison to **?** (only 129 nearby galaxies though)

CH: limitations of DEM and potential improvements

- too many luminous galaxies
- color distribution isnt' perfect.
- There isn't a whole lot of flexibility for SFR=0 galaxies predicted by simulations and they do not agree well with observations A.

CH: How robust are our results? We fix the UV bump to reduce the number of parameters. But when run our analysis without fixing the UV bump, we find it does not impact our results. We also get no constraints on the UV bump parameters.

We rely on the slab model. But nothing changes when we use a more flexible truncated normal distribution in Appendix B. tnorm DEM model allows us to also vary the scatter of the attenuation curve

CH: How about our prior choice?

CH: restate what we learn about dust through DEMs paragraph on restating how we can learn about dust through DEMs based on trends we see across all simulations. summarize main findings again.

CH: If we marginalize over dust, can we learn anything about galaxy evolution from the simulation?

Are there observables that hydro sims + DEMs cannot reproduce? What does that say about the hydro sims?

What observables are unaffected by DEMs? We should chase those observables.

We clearly have to becareful with overinterpreting hydro sims because modifying dust allows us to reproduce whatever we want.

- Should we bother calibrating our empirical and semi-analytic models to hydrodynamic simulations when the hydro sims also require marginalizing over dust parameters? Does this mean that if our goal is to make realistic mocks, we can be relatively careless about

CH: What are some applications for DEMs? Realistic mock catalogs that reproduce observations in observable-space rather than physical parameter space.

5. SUMMARY

ACKNOWLEDGEMENTS

It's a pleasure to thank ... This material is based upon work supported by the U.S. Department of Energy, Office of Science, Office of High Energy Physics, under contract No. DE-AC02-05CH11231. This project used resources of the National Energy Research Scientific Computing Center, a DOE Office of Science User Facility supported by the Office of Science of the U.S. Department of Energy under Contract No. DE-AC02-05CH11231.

APPENDIX

A. RESOLUTION EFFECTS

Figure demonstrating imprint SFR=0 leave on the observable space and how we deal with them so we can ignore them...

B. BEYOND THE SLAB DEM

A major assumption of our fiducial DEM is that we sample the amplitude of attenuation from the slab model. The slab model makes the simplifying assumption that dust in galaxies are in a slab-like geometry and illuminated by the stellar radiation source (Somerville & Primack 1999). Then, for a given τ_V, the attenuation depends solely on the orientation of the galaxy. This simplification, ignores any complexities in the star-to-dust geometry that impact the shape of the attenuation curve (Witt Gordon 1996, 2000, Seon Drain 2016). TODO

Besides its simplifications, the slab model predicts A_V distribution with significant differences than the A_V distributions measured from observations. In Figure 8, we compare the A_V distribution predicted by the slab model (black) to the A_V distribution of star-forming galaxies in our SDSS sample (blue). The A_V values are derived using SED fitting from the **?** MPA-JHU catalog and how are the SF galaxies classified. The slab model A_V values are derived using Eq. 3 and 4 with M_*s and SFRs from the same SDSS sample and the inclinations, i, are uniformly sampled over the range TODO

$[0, \pi/2]$. With $\{m_{\tau,1}, m_{\tau,2}, c_\tau\}$ chosen to reproduce the observed A_V distribution, the slab model can reproduce the overall shape. However, it predicts an extended high A_V tail not found in observations.

Given these shortcomings of the slab model, we want to ensure that our results do not hinge on the slab model. Modeling the star-to-dust geometries with increased complexities, however, would involve expensive hydrodynamic simulations and dust radiative transfer calculations (*e.g.* Narayanan et al. 2018)jonsson2006, rocha2008, natale2015,hayward smith2015,hou2017,trayford2020. We instead take an empirical approach and implement a flexible model for sampling A_V based on a truncated normal distribution: TODO

$$A_V \sim \mathcal{N}_T(\mu_{A_V}, \sigma_{A_V}) = \frac{\mathcal{N}(\mu_{A_V}, \sigma_{A_V})}{1 - \Phi\left(-\frac{\mu_{A_V}}{\sigma_{A_V}}\right)}. \tag{B1}$$

Here, $\mathcal{N}$ is the standard normal distribution and $\Phi(x) = \frac{1}{2}\left(1 + \mathrm{erf}(x/\sqrt{2})\right)$ is the cumulative distribution function of $\mathcal{N}$. μ_{A_V} and σ_{A_V} are the mean and variance of the truncated normal distribution. Similar to Eq. 4, we allow μ_{A_V} and σ_{A_V} to depend on the physical properties of galaxies:

$$\mu_{A_V} = m_{\mu,1}(\log\ M_* - 10.) + m_{\mu,2} \log\ \mathrm{SFR} + c_\mu \tag{B2}$$

$$\sigma_{A_V} = m_{\sigma,1}(\log\ M_* - 10.) + m_{\sigma,2} \log\ \mathrm{SFR} + c_\sigma. \tag{B3}$$

The A_V distribution from our truncated normal (orange dashed) closely reproduces the observed SDSS A_V distribution (Figure 5). N_T is able to reproduce the overall skewness but unlike the slab model, it does not have a long high A_V tail. With more free parameters and a functional form that closely resembles the observed A_V distribution, the truncated normal model provides a flexible altnerative to the slab model and we include it in our analysis.

REFERENCES

Abazajian K. N., et al., 2009, The Astrophysical Journal Supplement Series, 182, 543

Baes M., Trčka A., Camps P., Nersesian A., Trayford J., Theuns T., Dobbels W., 2019, arXiv:1901.08878 [astro-ph]

Battisti A. J., Calzetti D., Chary R.-R., 2016, The Astrophysical Journal, 818, 13

Battisti A. J., Calzetti D., Chary R.-R., 2017, The Astrophysical Journal, 840, 109

Blanton M. R., Roweis S., 2007, The Astronomical Journal, 133, 734

Blanton M. R., et al., 2005, The Astronomical Journal, 129, 2562

Buat V., et al., 2005, The Astrophysical Journal Letters, 619, L51

Burgarella D., Buat V., Iglesias-Páramo J., 2005, Monthly Notices of the Royal Astronomical Society, 360, 1413

Calzetti D., 2001, New Astronomy Reviews, 45, 601

Camps P., Baes M., 2015, Astronomy and Computing, 9, 20

Chabrier G., 2003, Publications of the Astronomical Society of the Pacific, 115, 763

Garn T., Best P. N., 2010, Monthly Notices of the Royal Astronomical Society, 409, 421

Hahn C., Vakili M., Walsh K., Hearin A. P., Hogg D. W., Campbell D., 2017, Monthly Notices of the Royal Astronomical Society, 469, 2791

Iglesias-Páramo J., et al., 2006, The Astrophysical Journal Supplement Series, 164, 38

Ishida E. E. O., et al., 2015, Astronomy and Computing, 13, 1

Kriek M., Conroy C., 2013, The Astrophysical Journal Letters, 775, L16

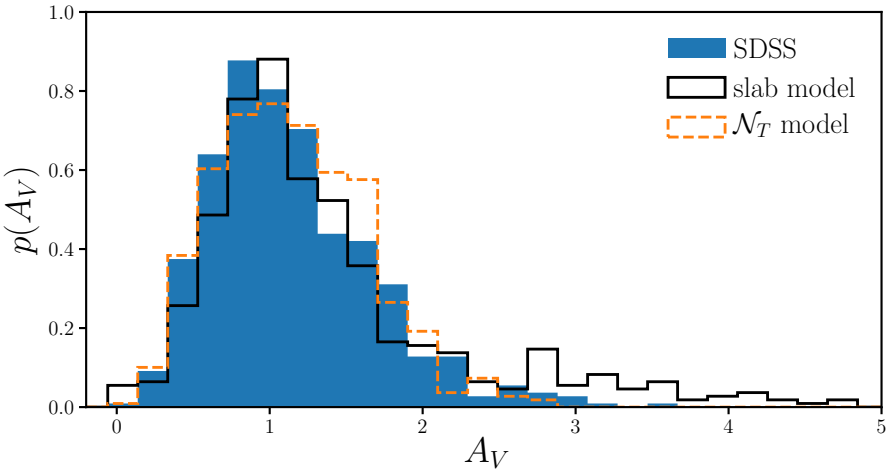

Figure 8. Comparison of A_V distribution of SDSS star-forming galaxies (blue) to predictions from the slab model (Eq. 3; black). detail on how SDSS SF galaxies are classified. The slab model assumes that there's a slab of dust in front of a galaxy. We use $\tau_V = 2$ for the slab model above. Regardless of τ_V, however, the slab model predicts a significantly more asymmetric and peaked A_V distribution than observations. Given this disagreement, *we include in our analysis a DEM with an empirical prescription for A_V based on a truncated normal distribution, which better reproduce the observed A_V distribution* (Section B).

Narayanan D., Conroy C., Davé R., Johnson B. D., Popping G., 2018, The Astrophysical Journal, 869, 70

Nelson D., et al., 2018, Monthly Notices of the Royal Astronomical Society, 475, 624

Noll S., Burgarella D., Giovannoli E., Buat V., Marcillac D., Muñoz-Mateos J. C., 2009, Astronomy and Astrophysics, 507, 1793

Salim S., Narayanan D., 2020, arXiv:2001.03181 [astro-ph]

Salim S., Boquien M., Lee J. C., 2018, The Astrophysical Journal, 859, 11

Somerville R. S., Primack J. R., 1999, Monthly Notices of the Royal Astronomical Society, 310, 1087

Somerville R. S., Gilmore R. C., Primack J. R., Domínguez A., 2012, Monthly Notices of the Royal Astronomical Society, 423, 1992

Tinker J., Wetzel A., Conroy C., 2011, preprint, 1107, arXiv:1107.5046

Tinker J. L., Hahn C., Mao Y.-Y., Wetzel A. R., Conroy C., 2018, Monthly Notices of the Royal Astronomical Society, 477, 935

Trayford J. W., et al., 2015, Monthly Notices of the Royal Astronomical Society, 452, 2879

Trayford J. W., et al., 2017, Monthly Notices of the Royal Astronomical Society, 470, 771

Trayford J. W., Lagos C. d. P., Robotham A. S. G., Obreschkow D., 2020, Monthly Notices of the Royal Astronomical Society, 491, 3937

Tress M., et al., 2018, Monthly Notices of the Royal Astronomical Society, 475, 2363